

EFFECT OF CHEMICAL COMPOSITION ON THE ELECTROCHEMICAL AND WEAR BEHAVIOR OF BORON CARBIDE REINFORCED COPPER COMPOSITES

T. Albert^{1,2*}, D. Prince Sahaya Sudherson³, K. Kalaiselvan⁴ and N. Leema⁵

¹Department of Mechanical Engineering, Anna University, Chennai, Tamil Nadu 600 025, India

²Department of Mechanical Engineering, V. V. College of Engineering, Tisaiyanvilai, Thoothukudi, Tamil Nadu 628 656, India

³Department of Mechanical Engineering, Rohini College of Engineering and Technology, Palkulam, Kanyakumari, Tamil Nadu 629 401 India

⁴Department of Mechanical Engineering, Oasys Institute of Technology, Pulivalam, Tiruchirapalli, Tamil Nadu 621 006 India

⁵Department of Computer Science & Engineering, Chitkara University Institute of Engineering & Technology, Chitkara University, Punjab 140 401, India

(Received January 9, 2023; Revised February 22, 2023; Accepted February 23, 2023)

ABSTRACT. In this work, the Copper composites Cu-x wt. % B₄C (x = 0, 5, 10, 15, 20) were fabricated for the metallurgical and mechanical property evaluation as per ASTM standards. The metallurgical characterization tests on the samples include x-ray diffraction, optical microscopy, and scanning electron microscopy with EDX. Further, pin-on-disc apparatus was used to investigate the tribological behavior of composite specimens. An SEM micrograph of the worn surface and wear debris, along with the Gwyddion software, has been used to discuss the wear mechanisms in detail. The Artificial Neural Networks (ANN) classifier model is also constructed to describe the wear behavior in more detail. The experimental results inferred that the addition of Boron carbide particles has enhanced the Copper's corrosion resistance in a 1 M HCl electrolyte solution from 30.34% to 74.2%, 75.08%, and 83.29% with B and C ions. Also, it significantly enhance the mechanical and tribological characteristics considerably.

KEY WORDS: Powder metallurgy, Cu-B₄C, Gwyddion, Wear, Artificial Neural Network

INTRODUCTION

Metal matrix composites (MMCs) have undergone extensive research in recent years to significantly improve the manufacturing of numerous complicated shapes with varying compositions. MMCs are the ideal combination of metals and ceramics that can improve the characteristics of various materials. It can be produced using either the liquid or solid state, with powder metallurgy under the latter. Porosity, wettability, and the chemical reaction between the matrix and reinforcement with the atmosphere are the main obstacles to the liquid metallurgical approach. It's challenging to achieve a uniform distribution of the metals in a molten condition [1, 2]. Powder metallurgy (PM) is one of the most advanced, adaptable, and simple techniques, where complex components can be produced by effectively controlling the composition. Potential benefits include enhanced strength due to the homogeneous distribution of reinforcing particles, cost-effective bulk production, close tolerances and near-net shape components [3-9]. Electrical and optical industries generally depend on copper because of its good electrical conductivity and corrosion resistance [9, 10].

Pure copper had notably poor mechanical and wear characteristics at low and high temperatures. According to Zhan *et al.* [11] and Prajapati *et al.* [3], the reinforcement added influences property enhancement. In order to significantly improve the characteristics of copper,

*Corresponding author. E-mail: albert@vvcce.org

This work is licensed under the Creative Commons Attribution 4.0 International License

reinforcement particles such as TiC [11, 12], SiC [13, 14], W [15, 16], B₄C [17], TiB₂ [18], and Fly ash (FA) [19, 20] can be added. In general, variables including weight percentage, volume percentage, particle size, interfacial bonding, aspect ratio, and reinforcement orientation had an impact on composites. The combined corrosion resistance of copper tungsten alloys made them ideal for nuclear and power applications [21, 22]. A decrease in wear and friction of the sliding pair was seen as the amount of graphite in the compound increased [22, 23]. Wang *et al.* [24] established the hardness values for copper 0.5% graphene composite (Cu-0.5GN) and Cu-graphite composite at 650 °C. Diffusion of atoms across the grain boundaries caused the values of Cu-0.5 GN to be twice as high as those of Cu-G. To increase the low coefficient of friction and poor machinability of fine graphite, copper fly ash composites were used as reinforcement [25].

Ceramic material such as boron carbide (B₄C) is the third toughest material (2900-3900 kg/m²), followed by diamond and boron nitride [26, 27]. B₄C was used to reinforce and improve the wear characteristics, thermal conductivity, high modulus of elasticity, and hardness of metal matrix composites. When the B₄C level in AA2014 alloy increases, density and ductility decrease, respectively [28]. As the amount of aluminium in the Al-B₄C composite increases, the tensile strength keeps increasing [29]. When the reinforcing content has increased by 50% vol., the Mg-B₄C composite's hardness increases compared to pure magnesium [29]. According to Arumugam *et al.* [30], the Artificial Neural Network (ANN) technique can predict the tensile specimen's ultimate tensile strength. The ANN-based model was developed by Vettivel *et al.* more precisely analyze the tribological properties of Cu/W composite [31]. The same ANN-based model was used to assess mechanical and tribological characteristics, such as hardness, specific wear rate, and COF. Although only some researchers have studied copper-based MMCs via the PM approach, no one has reported on the mechanical, tribological, and wear debris surface roughness of Cu-B₄C composites using Gwyddion software. Furthermore, no research involving wear behavior and classifier-based ANN modeling has been described. Hence a novel attempt is made to investigate the behavioral changes.

EXPERIMENTAL

The Cu-B₄C MMCs with different compositions were prepared using pure copper and B₄C powders. The powder samples were of the same mesh size (20 to 30 microns) for uniform blending. Copper and boron carbide powders were tested for particle size in a wet environment using a Malvern master sizer 2000, version 6.0. Particle dispersion and deagglomeration were prevented by using an ultrasonic treatment for 60 seconds. Copper and B₄C powder were taken separately and blended on different calculated weight percentages (0, 5, 10, 15 and 20%). The powder mixture was blended for 4 hours at 350 rpm using a small planetary ball mill in smart systems. Blending was done using titanium carbide balls, maintaining a 10:1 ball-to-powder weight ratio. The powder compaction die, which has a 15 cm diameter and 30 cm height, is filled with homogeneously mixed Cu-B₄C powder. The blended powder, weighing 80 g, is cold compacted in a 100-ton BEMCO hydraulic press at a force of 240 kN. The die walls are lubricated with graphite before each run. In accordance with MPIF 42 standards, the green density of 85% was maintained. Green compacts were sintered on the muffle furnace after being ejected from the die set. In an argon environment, sintering took place for two hours at 950 °C. The sintered specimens were allowed to cool in the furnace until room temperature.

The prepared specimens were cleaned with a wire brush and then machined in accordance with guidelines for material characterization investigations. X-ray diffraction (XRD) was performed on the varied composition specimens to determine the composite's components, phases, and particles. The testing was carried out in the powdered samples from 20 to 90 degrees in X'Pert PRO, Holland. The micro-structural examination was carried out using conventional metallographic techniques. Specimens were carefully polished on the SiC papers from 80 to 1500 grit, with diamond pastes of 3µm and 0.3µm in velvet cloth to remove the scratches and obtain a mirror finish. Finely polished specimens were etched with 20 ml HNO₃ and 90 ml distilled water.

Microstructural studies were carried out with the help of an Olympus optical microscope. Hardness measurement was done on a Vickers hardness tester [Mitutoyo], adhering to ASTM-384 standards. Electrical conductivity measurement was done with the help of a four-point probe tester for pure Cu and different B₄C added composites. Electrical conductivity is the reciprocal of electrical resistivity ($\rho = RA/L$ where R- resistance, A- area of the specimen and L- length of the specimen). Electrical resistivity was measured under a nitrogen atmosphere at 0.5 Amp current with different temperatures. Thermocouples are utilized to change the temperature. Density measurement was done as per the ASTM B962-13 standards. After cutting the Cu-x wt. % B₄C (x = 0, 5, 10, 15, 20) into a 1 cm by 5 cm square specimen, the sample was polished with 1000 grit emery paper and cleaned in an ultrasonic bath containing a mixture of acetone and water. Before undergoing electrochemical corrosion investigation, the specimens were dried in a hot air oven at 80°C for 30 minutes. A Tafel plot, overpotential-logarithmic current density connection was extrapolated to get the Tafel slope, corrosion current density, and corrosion potential.

The wear experiment was conducted for 3 trials with normal loads of 20, 40, and 60 N, a standard sliding speed of 1 m/s, and a maximum sliding distance of 1800 m. The surface morphology of the wear debris is analyzed through Gwyddion 2.61 software, generic software for data visualization and analysis. The effect of the scanning speed and the spacing in a roughness measurement was studied on the reference specimen using the "TALYSURF CLI 1000" Profilometer. It was done using a Gaussian filter with an 800 m pore size and a microfiltration ratio of 2.5 m. The data was analyzed using the "Taly Map Platinum" software. A scanning electron microscope (ZEISS Gemini SEM 300) was used to examine the blended powders, the finished composite's worn surface and the wear debris of each specimen. An artificial neural network (ANN) is simulated on the Matlab-2021b platform, which is used to validate and optimize.

RESULTS AND DISCUSSION

Figure 1(a, b) shows a mono-modal, mono-dispersed material. Obscuration values for Cu and B₄C were 10.56 and 11.27 percent, respectively. The acceptable range of obscuration for a Malvern Optimizer 2000 is 10 to 20 %. SEM images of Cu, B₄C and thoroughly blended Cu-B₄C particles are shown in Figure 1(c-e). The micrograph confirms the size and distribution of the particles in the sample. Both smooth-edged dendritic copper and sharp-edged B₄C particles can be seen in Figure 2(c) [2]. Particle size distribution (PSD) of pure copper and B₄C powder was analyzed before blending and the conditions of experimentation are listed in Table 1.

Table 1 Particle size distribution analysis results of Cu, B₄C powders.

Description	Cu powder	B ₄ C powder
Refractive index	1.100	1.570
Dispersant refractive index of water	0.737	1.330
Specific surface area	0.0455 m ² /g	0.112 m ² /g
Concentration uniformity	0.5065	0.276

The density measurement results for the Cu-xB₄C, (x = 0, 5, 10, 15, 20) samples are 7.5, 7.14, 6.76, 6.21 and 5.66 g/cm³ respectively. As the density of B₄C is low than copper, the increased B₄C addition reduces the density of Cu-B₄C composite [17, 28, 32]. The void fraction of the fabricated composites was found to be less than 1. The composites electrical conductivity and resistivity were found to be 86.2, 83.5, 80.91, 77.87, 74.22 %IACS and 1.16, 1.19, 1.23, 1.28, 1.34x10⁻⁸ Ωm, respectively. The electrical conductivity decreases with the addition of B₄C particles; normally, the conductivity of pure copper is more than powder composites due to their porosity [3]. The fabricated composites are used in the manufacturing of electrical relays and switches. The conductivity was found to decrease as the percentage of reinforcement increased

similar effect is reported by Yener *et al.* [27]. Moreover, the electrical resistivity of the composites increases as the hard B_4C particles addition is increased, which disrupts the current flow.

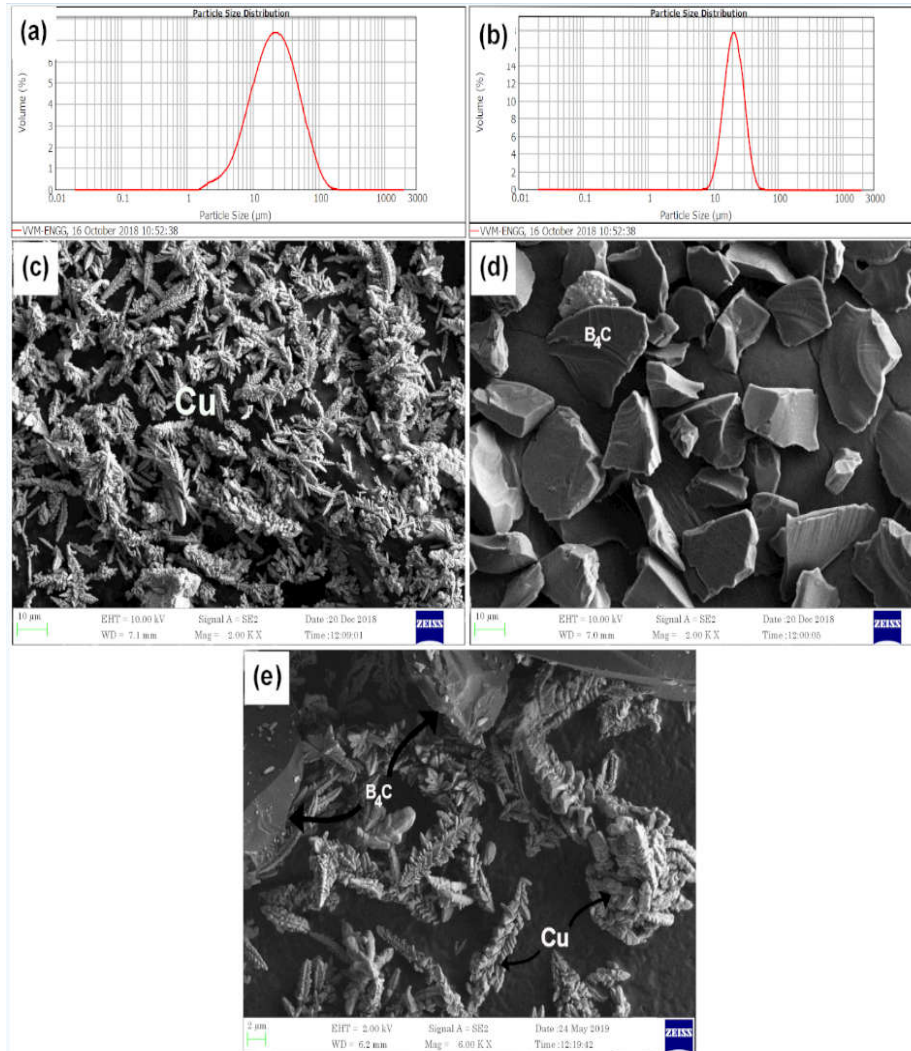


Figure 1. (a-b) Particle size distribution analysis and (c-d) SEM of Cu and B_4C particles and (e) SEM Cu- B_4C blended powder.

The X-ray diffraction (XRD) results are shown in Figure 2; the absence of Cu_2O peaks indicates the samples produced are defect-free. The maximum intensity peaks for copper and boron carbide are located in the spectrum at the two theta values of 43.317° and 37.768° . The weak peak of B_4C is due to the lower volume addition of B_4C into the copper matrix [5]. SEM results of the randomly chosen compositions (Cu-5 B_4C and Cu-15 B_4C) are shown in Figure 3 (a, b). The dark-color angular-edged B_4C particles are indicated on the grey colour copper matrix

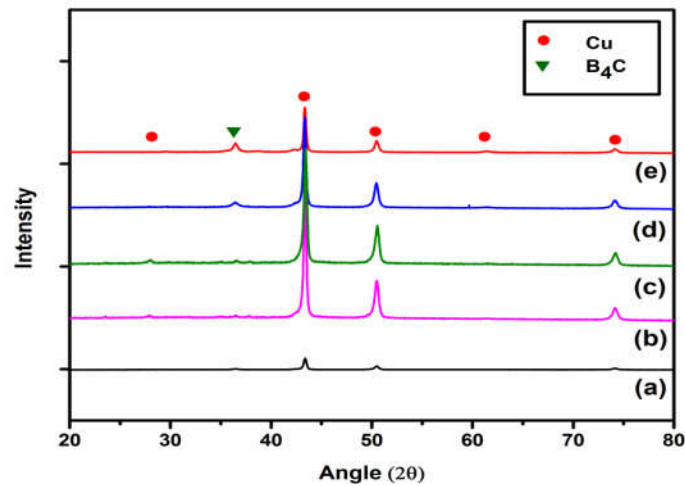


Figure 2. XRD results of composites (a) Cu, (b) Cu-5B₄C, (c) Cu-10B₄C, (d) Cu-15B₄C and (e) Cu-20B₄C.

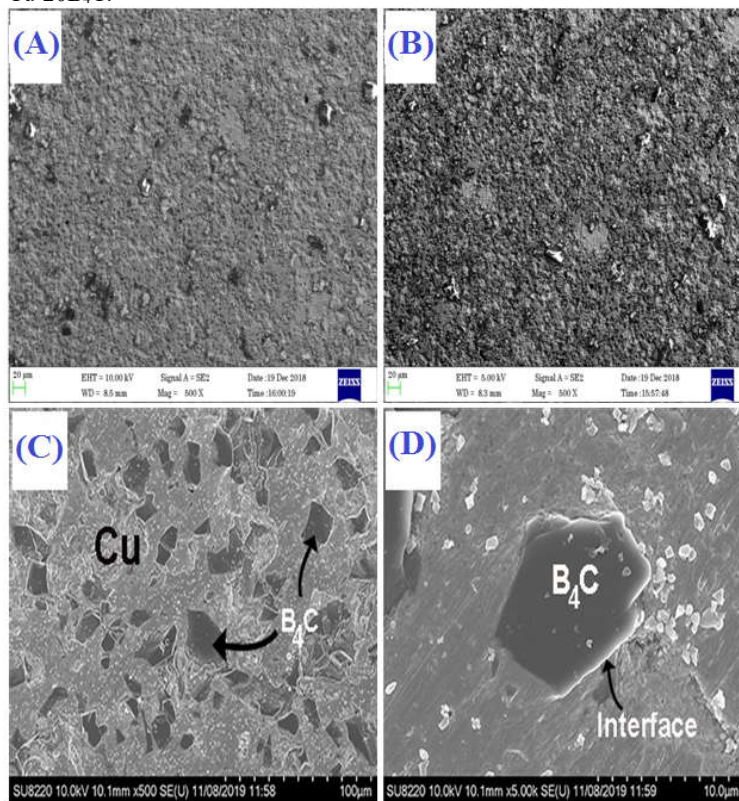


Figure 3. SEM image results (a) Cu-5B₄C, (b) Cu-15B₄C, (c) SEM (Point) of Cu-15B₄C and (d) SEM (Surface) of Cu-15B₄C.

region in the SEM micrographs [17]. Interfacial reactions are vital in accounting for composite material's mechanical and creep behavior. The interface can be influenced by composite material by sharing the load to matrix and reinforcement. The surface and point SEM results of Cu-15B₄C composites are shown in Figure 3(c-d). In the surface SEM, we can observe a homogeneous distribution of B₄C particles. Even though a close bond between Cu and B₄C particles is noticed in the Cu-B₄C interface, no chemical reaction is observed in Figure 3(d). Precipitate and reaction-free interface regions indicate superior integrity with the interfaces [33-38]. Elemental mapping results of Cu-15B₄C are shown in Figure 4 (a-e). Figure 4 (b-d) shows the elemental mapping images of Cu, B and C elements, respectively. Yellow, red and blue colored regions represent the presence of copper, boron and carbon particles, respectively.

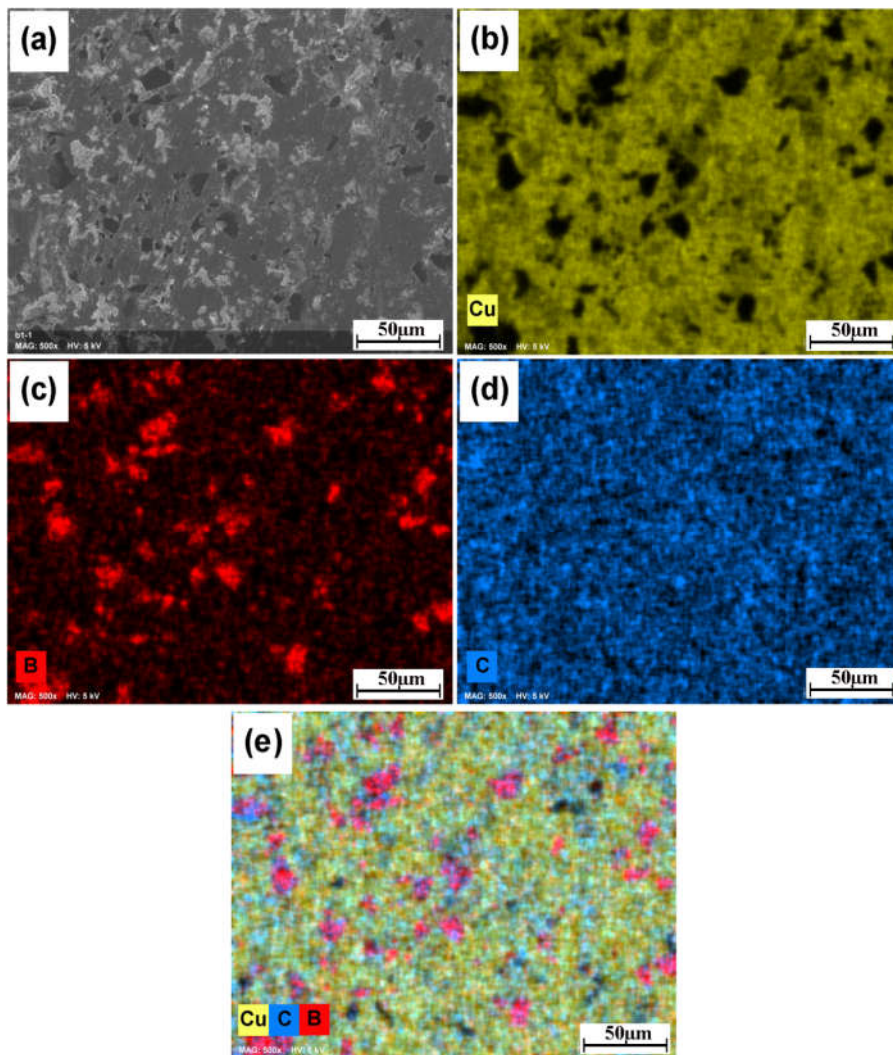


Figure 4. SEM-EDX mapping of Cu-15B₄ composite.

Samples of Cu-x wt.% B₄C (x = 0, 5, 10, 15, 20) are subjected to corrosion testing in 1M HCl to evaluate the material's resistance to corrosion in acidic, neutral, and basic conditions. The applied voltage is a gradual drop from -2 V at a rate of 0.5 mV/s to 0 V. All the copper samples began to electrochemically corrode at a value of -2 V. Potentiodynamic polarisation curves (or tafel plots) for Cu-x wt.% B₄C samples in 1M HCl electrolyte solution are shown in Fig. 5. It's a visual representation of how a metal's electrode potential affects the current produced by an electrochemical cell. The exchange current density is used as a measure of catalytic activity, while the Tafel slope sheds light on the reaction process. As opposed to pure copper, corrosion potential values of Cu-x wt.% B₄C (x = 0, 5, 10, 15, 20) are shifted to the positive side (anodic region).

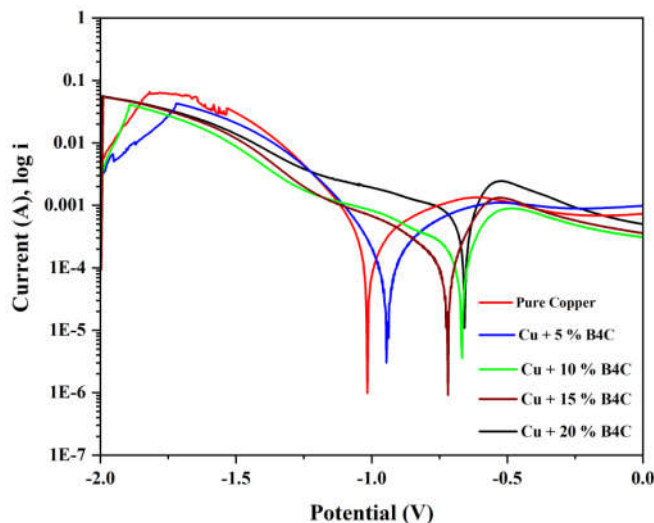


Figure 5. Tafel plots of the Cu-x wt. % B₄C (x = 0, 5, 10, 15, 20) specimens under three different electrolytes.

DC electrochemical corrosion study often uses potentiodynamic polarisation measurement (PDP). The high voltage supplied to the test electrode causes an oxidation or reduction process on the metal surface, generating a substantial current with PDPs (depending on the direction of polarisation). The polarisation curve may be calculated by connecting potential to current density (I, or log I) at each point. Under specific climatic conditions, a metal's polarisation curve may predict its corrosion rate (Tafel slope). The method's numerous benefits include precise corrosion detection, fast rate determination, easy corrosion prevention effectiveness assessment, etc.

Table 2. Potentiodynamic polarisation parameters of Cu-x wt.% B₄C (x = 0, 5, 10, 15, 20).

Sample	I _{corr} (x10 ⁻⁴ A/cm ²)	E _{corr} (V)	Polarisation resistance (Ω)	Corrosion rate (mm/yr)	Inhibition efficiency (IE) %
Pure copper	1.5674	-0.6599	87.928	1.8213	-
Cu + 5 % B ₄ C	1.0918	-1.0223	202.2	1.2687	30.34
Cu + 10 % B ₄ C	0.40292	-0.94268	445.43	0.46819	74.29
Cu + 15 % B ₄ C	0.37837	-0.66715	335.78	0.43966	75.08
Cu + 20 % B ₄ C	0.26183	-0.72091	416.28	0.30424	83.29

Parameters of potentiodynamic polarisation are tabulated in Table 2. They include the corrosion current (I_{corr}), the polarisation resistance, and the corrosion resistance. The calculated corrosion current (I_{corr}) for pure copper was 1.5674 A cm^2 , but the corresponding value for Cu-x wt.% B_4C ($x = 5, 10, 15, 20$) was only 0.4029 A cm^2 . In conclusion, the data provided above showed that pure copper specimens treated with B and C ions had better resistance to electrochemical corrosion and displayed a decreased corrosion rate. The addition of B and C ions increases copper's resistance to corrosion in a 1 M HCl electrolyte solution from 30.34% to 74.2%, 75.08%, and 83.29%, respectively, compared to untreated metal. In Figure 6, we examine the AC impedance of a composite electrode composed of Cu-x wt.% B_4C ($x = 5, 10, 15, 20$) in further detail as the results of an open-circuit test (inset).

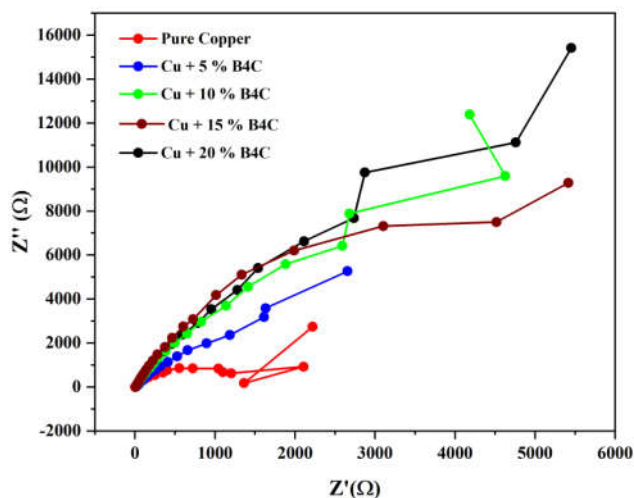


Figure 6. Impedance of a composite electrode composed of Cu-x wt.% B_4C .

As if it were sliced in half, the Nyquist plot may be seen in a different light. To visualise the imaginary and real parts of the complex impedance of individual electrodes or electrochemical cells, an electrochemical impedance spectroscopist creates a so-called Nyquist plot. Frequency-dependent real and imaginary components of a Fourier transform (FRF) are shown on the complex plane. Using the Nyquist plot, which is comprised of a semicircle curve with two intersecting points for the real axis (Z'), values of solution resistance (R_s) obtained from the first intercept point, closer to the origin, and the value of total resistance ($R_s + R_{\text{ct}}$) obtained from the second intercept point, further from the origin, is possible because of the symmetry of the complex plane and the circularity of a FRF. Curved at high frequencies owing to charge transfer resistance, the Cu-x wt.% B_4C composite electrode exhibits straight behaviour at low frequencies due to its EDLC behaviour. The low internal resistance of the composite electrode, as demonstrated when the curve was intercepted at low impedance, may contribute to the excellent specific capacitance performance of the Cu-x wt.% B_4C electrode.

A pin-on-disc wear tester provides the height loss data due to the wear of the specimen directly. The hardness and workability of composite materials depend on the height loss. Height loss for pure copper is high and decreases for the reinforced composites, as shown in Figure 7(a). The height loss data are directly obtained from the results. The loss of volume per unit meter of sliding distance is known as wear rate [39-41]. Wear rate (W) is calculated using where “ dV ” is worn volume in mm^3 and “ dL ” is the distance of sliding (m). In the wear test, sliding distance can

be calculated by knowing the sliding speed and time. The rate of wear on different B₄C reinforced copper specimens is presented in Figure 7(b). The applied load is varied in three levels by maintaining a constant sliding speed of (1 m/s). The wear rate decreases as the reinforcement percentage increases irrespective of the load applied. Sathish *et al.* [42] found a low wear rate for the high hardness material. Similarly, the Cu-B₄C composite offers a low wear rate due to hard B₄C particles in the copper matrix [15]. Wear resistance of various percentages of B₄C addition concerning normal load is represented in Figure 7(c). Composites volume of secondary phases determines the resistance to wear. Asl *et al.* [43] reported that secondary phases could be introduced in the matrix to improve the wear resistance.

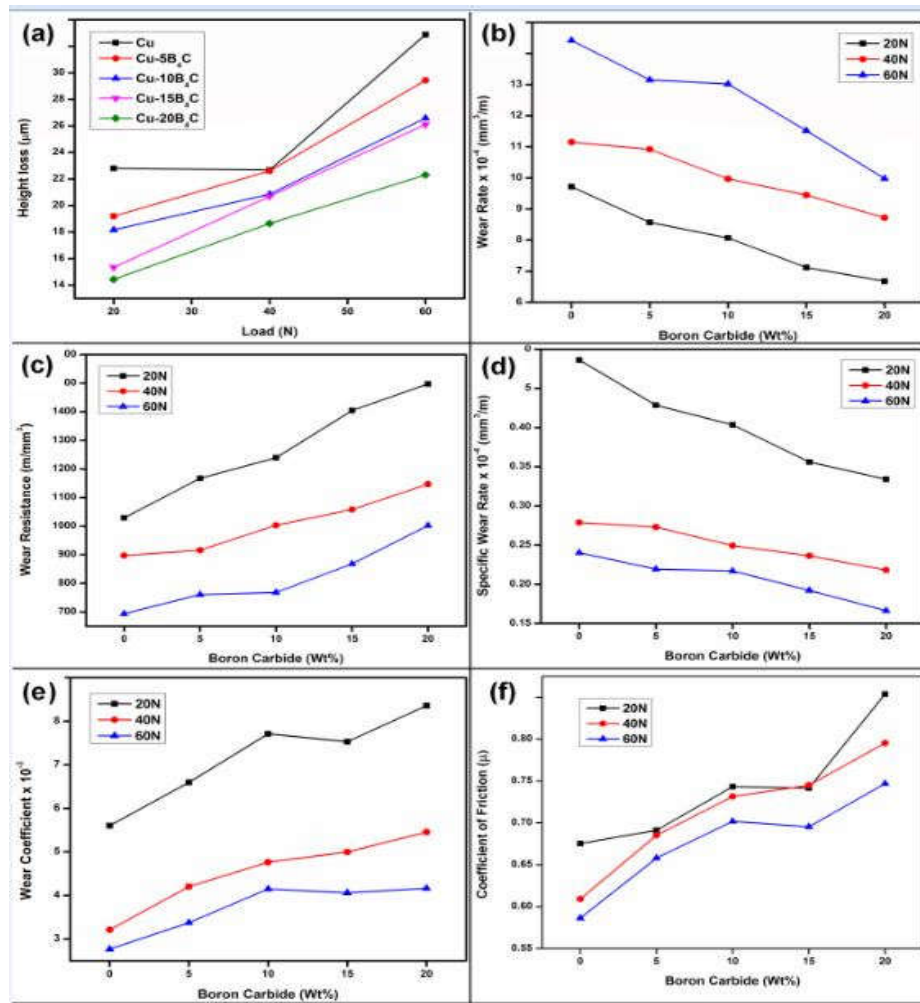


Figure 7. Wear behavior of composites (a) height loss, (b) wear rate, (c) wear resistance, (d) specific wear rate, (e) wear coefficient and (f) coefficient of friction.

The wear properties can vary by varying the type of matrix binding, quantity and phase of reinforcement. Wear resistance is calculated and measured in mm^3/m [44]. As the volume percentage of boron carbide increases, resistance to wear is increased due to the presence of the hard ceramic material. Dhokey *et al.* [45] predicted that with the increase of load, the wear resistance also increases. Specific wear rate is the ratio of wear rate to the load applied, which depicts the extent of load-bearing capacity. Normal load, sliding distance, and volume loss were the significant factors influencing the specific wear [39, 40]. Due to the increase in load, the work surface gets hardened; hence the specific wear rate reduces gradually [46]. The specific wear rate is inversely proportional to the normal load at a constant sliding distance. The specific wear rate decreases with the increase of sliding distance. The adhesive wear coefficients were calculated and the results were verified by Archard's equation [47, 48]. As per the Equation with the variation of the hardness value, the wear coefficient is also varied. Where "Ws" is the wear coefficient, "P" is the applied load, "V" is the volume loss by wear, "H" is the hardness of the specimen "L" is the sliding distance. Yang *et al.* [41] quantified the wear behavior and reported the coefficient of steady-state wear as a significant parameter. In Figure 7(e), the wear coefficient is increased with the increase in weight percentage of B₄C addition. Similarly, the wear coefficient decreases with the rise of the load applied. The wear rate is low when the wear coefficient is low; however, with the increase in weight percentage of reinforcement, the wear coefficient also increases [15]. The coefficient of friction [COF] between the mating surfaces is deduced from [49]. Figure 7(f) represents the graph of COF to the varied addition of B₄C under different normal loads applied. The COF of the Cu-B₄C composite is increased with the percentage increase of hard B₄C particles for all the normal loads. The COF is decreased when the applied load is increased due to the improved hardness.

The ANN simulation is performed to estimate the hardness, wear rate and COF concerning its height loss. The other parameters like load (20 N), sliding distance (2000 m) and surface area (25 mm^2) remain constant. The structure of the ANN has been designed using a multi-layer feed-forward with one hidden layer and the activation function used is logistic sigmoid to train the classifier. Levenberg-Marquardt's back propagation algorithm has been selected to train the ANN.

Step 1: Initialize the ANN structure with n input nodes, H hidden nodes and O output nodes. Where n is the number of input features and O corresponds to the number of class labels.

Step 2: Calculate the number of hidden nodes in the hidden layer using equation (1).

$$H = (2n + 1) \quad (1)$$

Phase 1: Feed Forward

Step 3: Calculate the output of each hidden node using Equation (2). Where y_j is the j -th hidden node, w_{ji} are the weights between the input and the hidden layer, x_i is the i -th input feature and θ_j is the bias value of the j -th hidden node.

$$f(y_j) = \frac{1}{(1 + \exp(-(\sum_{i=1}^n w_{ji}x_i - \theta_j)))} \quad j=1, 2, \dots, H \quad (2)$$

Step 4: Calculate the output of the output layer using Equation (3). Where z_k is the output class label and w_{kj} is the weights between the hidden and the output layer.

$$z_k = \sum_{j=1}^H w_{kj} f(y_j) \quad k = 1, 2, \dots, O \quad (3)$$

Step 5: Calculate Mean Squared Error (MSE) E_k using Equation (4). Where C_i^k is the target output and z_i^k is the network predicted output.

$$E_k = \sum_{i=1}^O (z_i^k - C_i^k)^2 \quad (4)$$

Step 6: Calculate Mean Absolute Percentage Error (MAPE) E_m using equation (5). Where N is the total input samples.

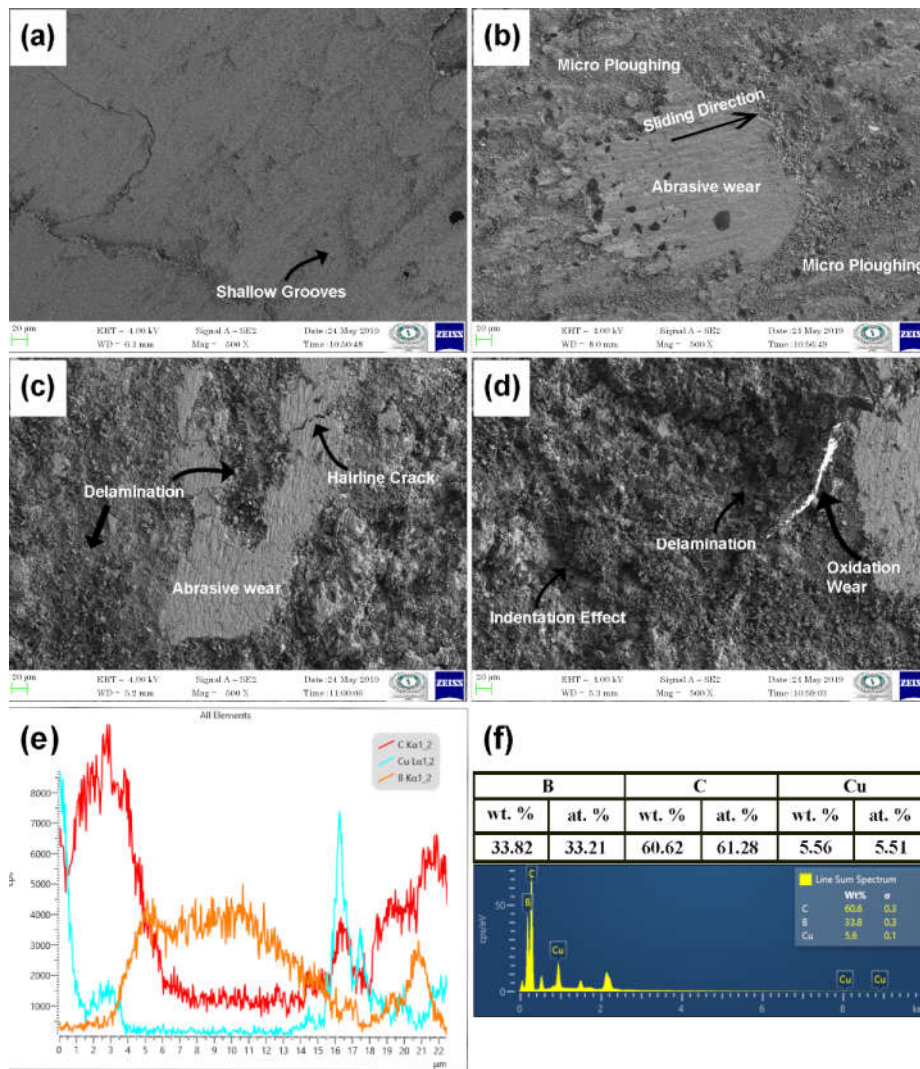


Figure 8. SEM micrographs of worn surface (a) Cu-5B₄C at 20 N, (b) Cu-5B₄C at 60 N, (c) Cu-20B₄C at 20 N, (d) Cu-20B₄C at 60 N and (e and f) EDS micrographs of Cu-20B₄C worn surface.

$$E_m = \frac{\sum |z_i^k - c_i^k|}{N} \times 100 \tag{5}$$

Phase 2: Backpropagation

Step 7: Compute the error in the network concerning the weights and biases using equation (6). Where η is the learning rate.

$$\Delta w_k = \eta(z_i - c_i)x_i \quad (6)$$

Step 8: Compute the error in the network concerning change in weights and biases using the Levenberg-Marquardt algorithm using Equations (7), (8) and (9). Where H' is the second derivative hessian matrix and g is the current gradient and J is the first derivative of the jacobian matrix.

$$\Delta w_k = -H'_k g_k \quad (7)$$

$$H' = J'J \quad (8)$$

$$g = J'E_k \quad (9)$$

In Figure 8(c), micro ploughing marks are visible in some places due to the plastic deformation of the matrix. Flow stress depends on the shear strain responsible for the material removal. A hairline crack at some regions in Figure 8(c, d) is due to the indentation effect of the hardened debris. Because of the non-uniform stress distribution on the worn surface, an irregularity in material removal is noticed. Small fragments of debris are observed on the worn surface due to the shallow grooves and ridges. EDX for the worn surface of Cu-20B₄C is shown in Fig. 8(e, f). The Line scan EDX plot is shown in Figure 8(e), similarly, in Figure 8(f) the elemental plot is evident to confirm the presence of elements like C, Cu and Boron on the wear surface. From EDS values we can be concluding the weight percentage of the materials along the scan line. A low cohesive force between the particles increases the wear rate at a higher load. Obtained result correlates the wear mechanism with delamination wear.

CONCLUSION

Various composition of copper boron carbide Cu-xB₄C (x = 0, 5, 10, 15 and 20) composites were produced via the powder metallurgy route. Microstructure, mechanical and tribological properties were investigated and summarized: (i) Boron carbide particles were homogeneously distributed on the copper matrix irrespective of the volumetric addition which is characterized through XRD, optical microscopy, scanning electron microscopy (SEM) and EDX results. (ii) The density and electrical conductivity of the Cu-B₄C exhibits a downward trend as the percentage addition of B₄C is increased. (iii) The addition of B and C ions increases copper's resistance to corrosion in a 1M HCl electrolyte solution from 30.34 % to 74.2%, 75.08%, and 83.29%, respectively, compared to untreated metal. (iv) The wear rate of Cu-B₄C composites decreases with the increase of B₄C addition. SEM reports of worn surface and wear debris authenticates the role of wear mechanisms like abrasive wear, delamination wear and oxidative wear on the Cu-B₄C composites. In addition, the profilometric studies also validate the wear studies.

A classifier-based ANN modeling is a cost-effective prediction of Cu-B₄C composites. The trained ANN for the Cu-B₄C composite with minimum MAPE and good agreement with experimental and predicted values.

REFERENCES

1. Hashim, J.; Looney, L.; Hashmi, M.S.J. Metal matrix composites: production by the stir casting method. *J. Mater. Process. Technol.* **1999**, *192*, 1–7.
2. Annigeri, U.K.; Veeresh, G.B. Method of stir casting of aluminum metal matrix composites: A review. *Mater. Today: Proc.* **2017**, *4*, 1140–1146.
3. Prajapati, P.K.; Chaira, D. Fabrication and characterization of Cu–B₄C metal matrix composite by powder metallurgy: Effect of B₄C on microstructure, mechanical properties and electrical conductivity. *Trans Indian Inst. Met.* **2019**, *72*, 673–684.
4. Tjong, S.C. Recent progress in the development and properties of novel metal matrix nano composites reinforced with carbon nanotubes and graphene nanosheets. *Mater. Sci. Eng. R: Report* **2013**, *74*, 281-350.

5. Altinsoy, I.; Efe, F.G.C.; Aytas, D.; Kilic, M.; Ozbek, I.; Bindal, C. Some properties of Cu-B₄C composites manufactured by powder metallurgy. *Period. Eng. Nat. Sci.* **2013**, *1*, 34-38.
6. Ravindran, P.; Manisekar, K.; Narayanasamy, P. Tribological properties of powder metallurgy – Processed aluminium self-lubricating hybrid composites with SiC additions, *Mater. Des.* **2013**, *45*, 561–570.
7. Murakami, R.; Matsui, K. Evaluation of mechanical and wear properties of potassium acid titanate whisker-reinforced copper matrix composites formed by hot isostatic pressing. *Wear.* **1996**, *201*, 193-198.
8. Sapate, S.G.; Uttarwar, A.; Rathod, R.C. Analyzing dry sliding wear behaviour of copper matrix composites reinforced with pre-coated SiCp particles. *Mater. Des.* **2009**, *30*, 376–386.
9. Surekha, K.; Els-Botes, A. Development of high strength, high conductivity copper by friction stir processing. *Mater. Des.* **2011**, *32*, 911–916.
10. Balamurugan, P.; Uthayakumar, M. Wear studies of copper-fly ash composite under dry sliding conditions. *Mater. Res. Express.* **2019**, *6*, 1065d5.
11. Yongzhong, Z.; Guoding, Z. The effect of interfacial modifying on the mechanical and wear properties of SiCp/Cu composites. *Mater. Lett.* **2003**, *57*, 4583–4591.
12. Buytoz, S.; Dagdelen, F.; Serkan I.; Mediha, Kok. Effect of the TiC content on microstructure and thermal properties of Cu–TiC composites prepared by powder metallurgy. *J. Therm. Anal. Calorim.* **2014**, *117*, 1277–1283.
13. Meydanoglu, O.; Jodoin, B.; Kayali, E.S. Microstructure, mechanical properties and corrosion performance of 7075 Al matrix ceramic particle reinforced composite coatings produced by the cold gas dynamic spraying process. *Surf. Coat. Tech.* **2013**, *235*, 108–116.
14. Efe, G.C.; Altinsoy, I.; Bindal, C. Effects of SiC on properties of Cu-SiC metal matrix composites. *Acta Phys. Pol. A.* **2012**, *121*, 251–253.
15. Vettivel, S.C.; Selvakumar, N.; Leema, N. Electrical resistivity, wear map and modelling of extruded tungsten reinforced copper composite. *Mater. Des.* **2014**, *56*, 791–806.
16. Ahuja, Y.; Ibrahim, R.; Paradowska, A.; Riley, D. Friction stir forming to fabricate copper–tungsten composite. *J. Mater. Process. Technol.* **2015**, *217*, 22–231.
17. Eski, O.; Islak, S.; Urayli, C. The effect of boron carbide amount on microstructure and electrical properties of Cu-B₄C composite materials. *Int. Conf. Adv. Mat. Manuf. Tech.* **2017**, 25-27.
18. Dinaharan, I.; Kalaiselvan, K.; Akinlabi, E.T.; Davim, J. Microstructure and wear characterization of rice husk ash reinforced copper matrix composites prepared using friction stir processing. *J. Alloy Compd.* **2017**, *718*, 150-160.
19. Babu, H.U.; Sai, N.V. Tribological properties of copper–flyash composite, *Int. J. Dev. Res.* **2013**, *3*, 001-004.
20. Balamurugan, P.; Uthayakumar, M. Influence of process parameters on Cu–fly ash composite by powder metallurgy technique. *Mater. Manuf. Process* **2015**, *3*, 313–319.
21. Gupta, S.; Singh, G. Copper graphite composite material fabrication and its mechanical properties. *Int. J. Adv. Res. Innov. Ideas Educ.* **2016**, *2*, 545-549.
22. Kovacic, J.; Emmer, S.; Bielek, J.; Kelesi, L.I. Effect of composition on friction coefficient of Cu–graphite composites, *Wear* **2008**, *265*, 417–421.
23. Zhan, Y.; Zhang, G. The effect of interfacial modifying on the mechanical and wear properties of SiCp/Cu composites. *Mater. Lett.* **2003**, *57*, 4583-4591.
24. Wang, Y.; Wang, H.Y.; Xiu, K. Fabrication of TiB₂ particulate reinforced magnesium matrix composites by two-step processing method. *Mater. Lett.* **2006**, *60*, 1533–1537.
25. Rajan, S.T.K.; Balaji, A.N.; Raghav, G.R.; Vettivel, S.C. Compression and corrosion behaviour of sintered copper-fly ash composite material. *Mater. Res. Express.* **2019**, *45*, 4–11.
26. Deepa, J.P.; Resmi, V.C.G. Studies on the influence of surface pre-treatments on electroless copper coating of boron carbide particles. *Appl. Surf. Sci.* **2011**, *257*, 7466–7474.

27. Yener, T.; Altinsoy, I.; Yener, S.C. An Evaluation of Cu-B₄C Composites Manufactured by Powder Metallurgy. *Acta Physica Polonica A* **2015**, *127*, 1045–1047.
28. Dwivedi, S.P. Microstructure and mechanical behaviour of Al/B₄C metal matrix Composite. *Mater. Today: Proc.* **2020**, *25*, 751-754.
29. Kevorkijan, V.; Skapin, S.D. Mg/B₄C Composites with a high volume fraction of fine ceramic reinforcement. *Mater. Manuf. Process.* **2009**, *24*, 1337–1340.
30. Arumugam, V.; Naren, R.; Sridhar, B.T.N. Ultimate strength prediction of carbon/epoxy tensile specimens from acoustic emission data. *J. Mater. Sci. Technol.* **2010**, *26*, 725-729.
31. Vettivel, S.C.; Selvakumar, N.; Leema, N. Experimental and prediction of sintered Cu–W composite by using artificial neural networks. *Mater. Design.* **2013**, *45*, 323–335.
32. Viswanath, A.H.; Dieringa, K.K.A. Investigation on mechanical properties and creep behavior of stir cast AZ91-SiCp composites. *J. Magnes. Alloy*, **2015**, *3*, 16-22.
33. Ipek, H.; Cuvalci, H.; Celebi, C. Tribological properties of boron carbide reinforced copper based composites. *Mater. Today: Proc.* **2017**, *2*, 102-107.
34. Filippov, A.V.; Khoroshko, E.S. Characterization of gradient CuAl–B₄C composites additively manufactured using a combination of wire-feed and powder-bed electron beam deposition methods. *J. Alloy Compd.* **2021**, *859*, 157824.
35. Alizadeh, M.; Alizadeh, M.; Amini, R. Structural and mechanical properties of Al/B₄C composites fabricated by wet attrition milling and hot extrusion. *J. Mater. Sci. Technol.* **2013**, *45*, 725–730.
36. Kalaiselvan, K.; Murugan, N.; Parameswaran, S. Production and characterization of AA6061–B₄C stir cast composite. *Mater. Des.* **2011**, *32*, 4004–4009.
37. Domnich, V.; Reynaud, S.; Haber, R.A. Boron carbide: Structure, properties, and stability under stress. *J. Am. Ceram. Soc.* **2011**, *94*, 3605–3628.
38. Kalaiselvan, K.; Dinaharan, I.; Murugan, N. Characterization of friction stir welded boron carbide particulate reinforced AA6061. *Mater. Des.* **2014**, *55*, 176–182.
39. Mandal, A.; Chakraborty, M.; Murty, B.S. Effect of TiB₂ particles on sliding wear behaviour of Al–4Cu alloy. *Wear* **2007**, *262*, 160–166.
40. Herbert, M.A.; Maiti, R.; Mitra, R.; Chakraborty, M. Wear behaviour of cast and mushy state rolled Al–4.5Cu alloy and in-situ Al_{4.5}Cu–5TiB₂ composite. *Wear.* **2008**, *265*, 1606–1618.
41. Yang, L.J. Wear coefficient equation for aluminium-based matrix composites against steel disc. *Wear* **2003**, *255*, 579–592.
42. Kumar, G.S.; Rajaguru, K. Evaluation of Al-C-B₄C composites fabricated by powder metallurgy for hardness and wear behavior. *Mater. Today: Proc.* **2020**, *78*, 45-56.
43. Asl, K.M.; Masoudi, A.; Khomamizadeh, F. The effect of different rare earth elements content on microstructure, mechanical and wear behavior of Mg–Al–Zn alloy. *Mater. Sci. Eng. A.* **2010**, *527*, 2027–2035.
44. Kumar, K.K.A.; Pillai, U.T.S.; Pai, B.C. Tribological behavior of Mg - Mg₂Si in-situ composite. *Mater. Sci. Forum.* **2012**, *710*, 401-406.
45. Dhokey, N.B.; Paretkar, R.K. Study of wear mechanisms in copper-based SiCp (20% by volume) reinforced composite. *Wear* **2008**, *265*, 117–133.
46. Kori, S.A.; Chandrashekharaiah, T.M. Studies on the dry sliding wear behaviour of hypoeutectic and eutectic Al–Si alloys. *Wear.* **2007**, *263*, 745–755.
47. Tayeb, N.E. The variation of hardness and wear coefficient in sliding wear of copper and aluminum alloys. *Wear.* **1994**, *174*, 63-69.
48. Lopez, A.J.; Rodrigo, P. Dry sliding wear behaviour of ZE41A magnesium alloy. *Wear* **2011**, *271*, 2836-2844.